Theoretical and experimental evidence of the role of electromagnetic resonance in the cleaning of nanotubes

A. G. Van der Geest,[1,2] K. E. Hurst,[2] N. D. Bronstein,[2] J. H. Lehman,[2] and M. T. Lusk[1]
[1]*Department of Physics, Colorado School of Mines, Golden, Colorado 80401, USA*
[2]*Optoelectronics Division, National Institute of Standards and Technology, Boulder, Colorado 80305, USA*
(Received 15 April 2009; revised manuscript received 15 February 2010; published 22 March 2010)

Amorphous carbon is removed from as-prepared, bulk, single-walled carbon nanotubes (SWCNTs) by illumination with a 248 nm (5 eV) excimer laser. The steps by which this occurs are explained using a combination of experiments and density-functional theory (DFT) calculations. We present measurements with a quartz-crystal microbalance and scanning electron microscope images as evidence of mass loss and morphological changes in proximity of the SWCNT material. DFT calculations are used to estimate the frequency-dependent, macroscopic dielectric constant. This is used to identify Mie resonances in the tubes which are generated by the 248 nm excimer laser. These resonances are responsible for local field enhancements that, in turn, increase the rate at which sp^2 bonds in the amorphous carbon are excited. The carbon is more easily oxidized from these excited states.

DOI: 10.1103/PhysRevB.81.115440 PACS number(s): 78.67.Ch

I. INTRODUCTION

Many of the envisioned applications for carbon nanotubes (CNTs) require the availability of raw material that is free of amorphous carbon (a-C) and metal catalysts.[1] However, common synthesis techniques, particularly arc discharge, also produce a large amount of non-nanotube content consisting of sp^2 (graphitic) and sp^3 (diamondlike) clumps in addition to CNTs.[2] Cleaning methods to remove this unwanted carbon, such as acid treatment, filtration, and size exclusion chromatography, have been the focus of significant effort.[3,4] However, each of these treatments either generates defects or is not scalable to mass production.[1,4]

It may be possible to develop an effective cleaning strategy using ultraviolet (UV) light from an excimer laser. The nature of the interaction of UV light and CNTs is distinct from that of other CNT-laser interactions at longer wavelengths. For example, Maehashi *et al.*[5] have shown that carbon nanotube enrichment can be achieved using lasers operating in the visible and near infrared. Ramadurai *et al.*[6] showed the structural evolution of bulk CNTs exposed to 10.6 μm laser light up to 15 kW/cm^2. UV cleaning has been demonstrated for 172 nm light through generation of ozone.[7] Experiments with UV lasers operating at common wavelengths such as 355,[8] 248,[9] and 193 nm (Ref. 10) are notable because CNTs, and other forms of carbon are characterized by an absorption spectrum having a broad Mie resonance centered near 248 nm (5 eV).[11] Yotani *et al.*[12] and separately Singh *et al.*[13] showed previously that multi-walled carbon nanotubes (MWCNTs) are structurally modified by exposure to 248 nm laser light. Separately, Hurst *et al.*[9,10] made the distinction that not all by-products of arc discharge are destroyed at the same rate. Furthermore, it is possible to remove a-C from the vicinity single-walled CNTs (SWCNTs) without changing the tube-diameter distribution and without changing the volume fraction of metal catalysts. Later, Hurst *et al.* showed that, in terms of effective cleaning, 248 nm works better than 193 nm, the presence of oxygen is preferred over nitrogen or vacuum, and ozone destroys a-C and CNTs alike.

In the present work, we investigate the electromagnetic (EM) interaction that leads to heating and photochemical processes at relatively low fluence. Our hypothesis is that the inherent dielectric properties as well as morphological structure of CNTs play a significant role in their cleaning. Specifically, we posit that a Mie resonance at 248 nm causes a local electric field enhancement that promotes oxidation. The field enhancement increases the rate of the $\pi \rightarrow \pi^*$ transition in the a-C in the vicinity of 5 eV (248 nm) (Ref. 14) while the $\pi \rightarrow \pi^*$ transition is at $\sim$4.6 eV (Ref. 15) in SWCNTs allowing for selective oxidation of the a-C. This transition is then expected to result in more non-nanotube carbon atoms in a state from which they can easily react with oxygen.[10]

Our approach draws on both experimental and computational analysis to elucidate the role of CNTs in the oxidation of unwanted carbon. Toward this end, experimental data is provided to show that CNT's significantly enhance the rate of oxidation. The computational work then provides an explanation for this. An isolated CNT is treated as a hollow, conducting cylinder and its local electric field strength is calculated in response to a polarized, monochromatic source. The analytical expression requires that the dielectric function be supplied and this is accomplished using density-functional perturbation theory (DFPT).[16,17] It is found that the 248 nm laser excites a Mie resonance in the tube which results in an enhanced local field strength. This Mie resonance is seen experimentally.[11,15,18–21] Amorphous carbon (a-C) is known to be photochemically active in this range[14] due to the $\pi \rightarrow \pi^*$ transition.[22,23] We therefore conclude that π bonds in the a-C neighboring conducting tubes are promoted to antibonding states at a greater rate than would be so without the tubes present.

II. EXPERIMENT

A. Experimental method

The present work considers SWCNTs produced by the arc-discharge method and sold commercially by Carbolex.[24]

It is claimed by the manufacturer and verified by others that Carbolex nanotubes have a diameter distribution approximately 1.4 nm and slightly smaller. This was verified by Raman spectroscopy and analyzing the radial breathing modes that are apparent in the range of 150–170 1/cm.[9] The present work includes additional experimental results with as-prepared Carbolex as well as control samples of a-C, graphite and graphite with metal. Samples of a-C, graphite, and nickel were obtained commercially and considered to be an approximation of the non-nanotube by-products contained in as-prepared Carbolex material. The best evidence for this approximation is documented by Raman spectroscopy from purity assessments by Landi *et al.* and thermogravimetric analysis (TGA) by Mansfield *et al.*[25]

The method of measuring mass loss using a quartz-crystal microbalance (QCM) for laser-induced damage is known.[26] In the present context, the measurements are analogous to TGA, whereby change in material content is correlated with mass loss.[25] The QCM technique measures shear-mode vibrations of an AT-cut quartz crystal and the relative mass changes are calculated by means of the Saubery equation.[26]

Previous Raman analysis has shown that the nanotubes are not destroyed preferentially based on diameter, as suggested by the distribution of the radial breathing modes.[9] Since smaller diameter nanotubes would be oxidized first due to their higher curvature[9,27] the constant distribution of the radial breathing modes with respect to the exposure suggests that the tubes are not oxidized. We therefore conclude that essentially no SWCNTs were destroyed in the cleaning experiments reported here. The scanning electron microscope (SEM) images offer qualitative support for this conclusion.

Two other experiments, similar to those discussed below, have recently been performed by Hurst *et al.*[28] Both of these were QCM experiments with either a sample of graphite or a sample of graphite mixed with 25% by weight nickel particles exposed to 248 nm light. The mass loss of these samples was shown to decrease at a higher rate for the first 15 s of exposure followed by a lower rates thereafter. The differences in mass loss between the pure graphite and graphite with metal mix were negligible when the mass of the metal was taken into account. This is expected to be due to the encapsulation of the particles in carbon and that the metal particle resonances are outside the frequencies of interest. The initial mass loss was attributed to the acoustic shock that accompanies the first pulse and the desorption of water and adsorbed atmospheric gases. If the initial mass loss is neglected then the results of Hurst *et al.*[28] show that the cleaning of graphitic material is relatively small and that the metal nanoparticles do not play a role in cleaning material from the sample.

Material samples for laser exposure were prepared in solution with chloroform and deposited on the QCM crystal by use of an air-brush technique described previously.[29] Scanning electron microscope images were acquired with a 20 kV accelerating voltage and in-lens detector with a 9 mm working distance to narrow the depth of field. An example of SWCNTs before laser exposure is shown in Fig. 2(a). Laser exposure consisted of 248 nm excimer laser beam with a pulse width of 20 ns and a repetition rate of 10 Hz. The beam

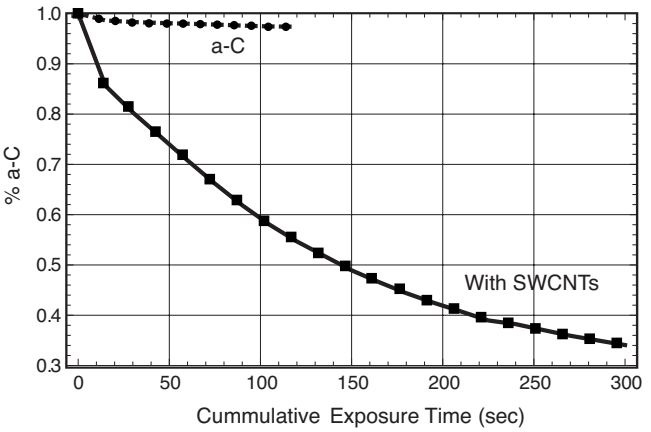

FIG. 1. Mass loss normalized by initial content of a-C for SWCNT (solid), a-C (dashed).

at the plane of exposure was a homogeneous square of approximately 1×1 cm^2 of randomly polarized light. The resonant frequency of the crystal was measured *in situ* by use of a SRS QCM 200 manufactured by Stanford Research. Each sample was exposed to 300 mW/cm^2 of UV light for 15 s intervals.

B. Experimental results

The experimental results are presented by plotting mass loss of representative samples on a QCM (Fig. 1) and imaging by SEM (Fig. 2). These results are not considered to be entirely sufficient for the present analysis. Our intention is to illustrate the evidence of the cleaning process while emphasizing our analytical conclusions. Our analysis considers earlier and pending experimental results documented elsewhere that include Raman spectrsocopy,[9] spectral responsivity,[9] QCM of graphite,[25] a-C, and a-C with metal, SEM, and TGA before and after laser exposure.[25]

The images shown in Fig. 2 present a qualitative picture of as-prepared SWNCTs before and after laser treatment. The contrast between images is that, following laser exposure, we observe fewer clumps of material surrounding well-defined threadlike structures that are presumed to be nanotube bundles. The postexposure SEM image in Fig. 2 supports the conclusion that nanotubes are not destroyed as indicated with Raman spectroscopy and the presence of radial breathing modes.[9]

The TGA experiments in this paper were performed in order to confirm the material content of the as-prepared Carbolex. Based on the mass of the residual material after oxidation to 800 °C, the amount of metallic impurities was 37% by weight. The amount of carbon impurities was determined from the derivative of the TGA. Two peaks centered at 377 and 447 °C represented the oxidation of amorphous and carbon nanotubes, respectively, in the sample. Based on analysis of the area under the curve, 50% by weight of the carbon content was SWCNTs, while the remainder was carbon impurities.

The plot shown in Fig. 1 depicts the change in mass of a-C remaining versus cumulative exposure time. The a-C

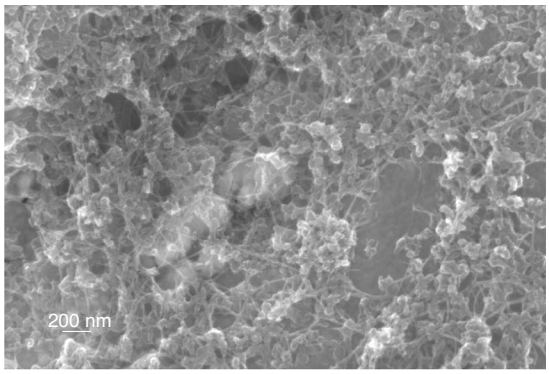

(a)

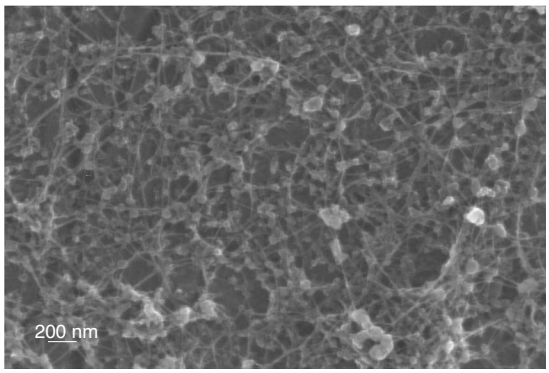

(b)

FIG. 2. An SEM image of as prepared SWCNT samples that are (a) unexposed or (b) exposed to 248 nm light.

exhibits losses 2.6% of its mass. This behavior is in contrast to mass loss on the SWCNT sample, with a reduction of nearly 65%. The decrease in mass following the first 15 s exposure is noteworthy. Dumont *et al.*[30] and Küper *et al.*[31] have investigated the interaction of 248 nm excimer laser light and photosensitivity on a QCM platform on the basis of a single pulse. The initial mass loss was attributed to a combination of the availability of superficial a-C, the desorption of water and other adsorbed atmospheric gases, and the acoustic shock that accompanies the first pulse.

III. CALCULATIONS

A. Idealized setting

A simple analytical model is constructed to elucidate the link between laser excitation and the removal of a-C. An electric field is incident on an isolated SWCNT idealized to be a hollow cylinder, as depicted in Fig. 3. The resulting field is then calculated and analyzed to determine the nature of any field enhancement attributable to the tube. The inner and outer radii are a and c, their average is b, and their difference is t,

$$a = b - \frac{t}{2}, \quad c = b + \frac{t}{2}. \tag{1}$$

The value of nanotube thickness, t, is taken to be the separation between two carbon sheets within graphite.

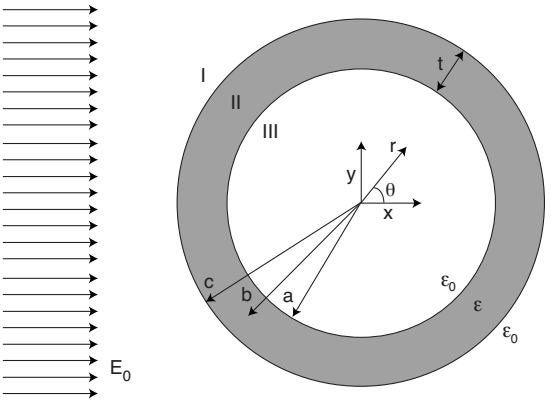

FIG. 3. Cross section of an idealized single-wall carbon nanotube.

The cylinder is endowed with a homogeneous, dispersive, relative dielectric function, ϵ, and is surrounded by vacuum. Its total charge density is assumed to be neutral. Since the surface enhancement effect arises due to a cross-sectional Mie resonance, the incident electric field polarization is taken to be within the cross-sectional plane of the nanotube, specifically the x direction. A quasistatic approximation is made because the wavelength of light is much larger than the diameter of the tube. Within this setting, the electric field can be calculated and its amplification in the vicinity of the tube quantified. A similar analysis was performed for bimetallic nanospheres by Wu *et al.*[32] The two-dimensional Laplace equation produces the electric potential for the three regions labeled in Fig. 3,

$$\varphi_{\mathrm{I}} = -E_0 r\cos(\theta) + \frac{(a-c)c^2(a+c)E_0(\epsilon-1)(\epsilon+1)}{a^2(\epsilon-1)^2 - c^2(\epsilon+1)^2}\frac{1}{r}\cos(\theta), \tag{2}$$

$$\varphi_{\mathrm{II}} = \left[\frac{2c^2E_0(\epsilon+1)}{a^2(\epsilon-1)^2 - c^2(\epsilon+1)^2}r + \frac{2a^2c^2E_0(\epsilon-1)}{a^2(\epsilon-1)^2 - c^2(\epsilon+1)^2}\frac{1}{r}\right]\cos(\theta), \tag{3}$$

$$\varphi_{\mathrm{III}} = \left[\frac{4c^2E_0\epsilon}{a^2(\epsilon-1)^2 - c^2(\epsilon+1)^2}r\right]\cos(\theta). \tag{4}$$

The potential shares a common denominator in all three regions and this allows resonant frequencies to be easily identified. All frequency dependence is embedded within the dispersive dielectric function. It is therefore the dielectric character that determines both the resonant frequencies and the resulting field enhancements in the vicinity of the nanotubes.

B. Dielectric functions

The approach used to determine the dielectric function, relies on an *ab initio* methodology in the form of DFPT. Calculations were performed on armchair (metallic) nanotubes ranging in a chirality from (3,3) to (12,12). All of the

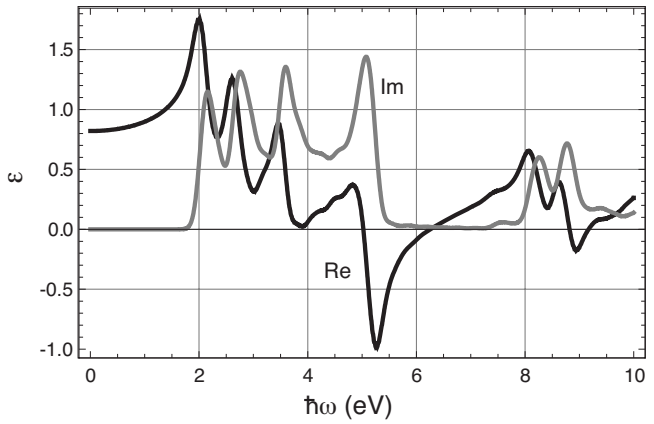

FIG. 4. The real (black) and imaginary (gray) components of the dielectric functions for a SWCNT generated from DFT for a (3,3) nanotube.

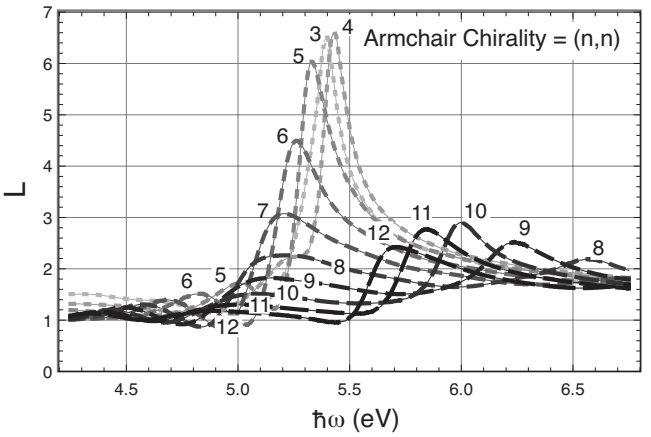

FIG. 5. $L(r_{\text{surf}}, \omega)$, at the surfaces of armchair CNTs of chirality (3,3) through (12,12). The diameter of Carbolex nanotubes is approximated by the diameter of (5,5), (6,6), and (7,7) nanotubes. While these tubes do not show largest enhancement, they do correspond in the range of 5 eV. DFPT tends to under estimate the position of absorption peaks (Refs. 38 and 39).

calculations were performed by use of the SIESTA DFT code.[16] The Troullier-Martin ultrasoft local-density approximation pseudopotential was employed with a double zeta basis set and a 200 meV energy shift. The convergence of the dielectric function was tested versus k points and resulted in the choice of a Monkhorst-Pack[33] k-point grid of dimension $1\times1\times70$.

For the DFPT calculation, incident light was polarized perpendicular to the length of the nanotube and a Gaussian broadening of 0.2 eV was assumed. The real and imaginary portions of the dielectric function for the (3,3) nanotube in Fig. 4 are consistent with literature values.[34] It is possible to further improve on this dielectric estimate since the approach does not fully capture the electron screening for $\hbar\omega<5$ eV. This is due to the local field effects of the polarization of light parallel to the nanotube.[35] However, Kramberger describes the local field effects as a mixing of transitions which play minimal role in the Mie resonance. Therefore the current level of accuracy was deemed sufficient to provide an understanding of the role that Mie resonances play in tube cleaning. It is also important to note that since the electromagnetic calculation of the electric field enhancement takes into account the shape effects of the nanotube including a spatial dependence in the dielectric function would be redundant. The dielectric from a DFT calculation is shown in Fig. 4.

The arc-generated SWCNTs discussed in the experimental section are known to form bundles of nanotubes therefore the effect of bundling on the dielectric function must be considered. Kataura showed in the first figure in his paper[18] that as prepared arc generated SWCNTs have two absorption peaks in the energy region ambiguously called the π plasmon centered on 4.6 and 5.2 eV. Since the generation method matches the method used for the Carbolex nanotubes used in this paper and Murakami[15] showed that one of the two peaks in SWCNTs is a surface-plasmon or Mie resonance it can be said that the Mie resonance still exists for bundled nanotubes. Also, for vertically aligned SWCNTs with small bundles Kranberger showed that a nondispersive peak with respect to momentum transfers existed as well as a peak with linear dispersion in the π plasmon region[19] which suggest the two peaks are a Mie resonance absorption peak and a electronic transition absorption peak.

Therefore several places in literature have shown that bundles of SWCNTs have two peaks in the π plasmon with one of these peaks being a Mie resonance. Since these articles show that the Mie resonance exists in bundled nanotubes the most likely form of interaction between the bundled nanotubes is that the Mie resonances will enhance the electric field from the neighboring SWCNTs. This effect is seen in silver nanoparticles and roughened silver surfaces in surface-enhanced Raman spectroscopy (SERS).[36,37] It is therefore reasonable to use the dielectric function of an isolated tube to study the Mie resonance with the understanding that the electric field enhancement will quite likely be higher in bundled tubes versus an isolated tube.

C. Electric field enhancement

A significant frequency-dependent field enhancement would help to explain the link between the presence of SWCNTs and cleaning efficiency. Two descriptions for the dielectric response are used to estimate field enhancement in proximity of SWCNTs. The induced electric field external to a cylinder, $\mathbf{E}_{\mathbf{ind}}$, can be determined from Eq. (2) using $\mathbf{E}=-\nabla\varphi$ and subtracting the incident field,

$$\mathbf{E}_{\mathbf{ind}}(r,\theta) = \frac{(a-c)c^2(a+c)(\epsilon-1)(\epsilon+1)}{a^2(\epsilon-1)^2-c^2(\epsilon+1)^2}\frac{E_0}{r^2}\cos(\theta)\hat{r} + \frac{(a-c)c^2(a+c)(\epsilon-1)(\epsilon+1)}{a^2(\epsilon-1)^2-c^2(\epsilon+1)^2}\frac{E_0}{r^2}\sin(\theta)\hat{\theta}. \tag{5}$$

The enhancement factor of the electric field, $L(r,\theta,\omega)$, is defined as the magnitude of the total electric field over the magnitude of the incident electric field,

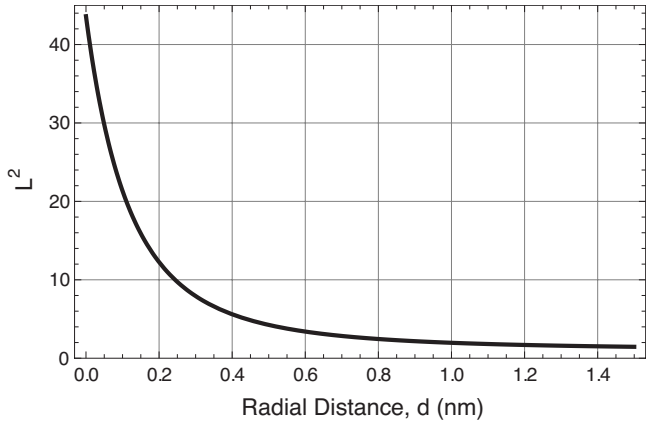

FIG. 6. $L(c+d,\omega)^2$, $\hbar\omega=5.4$ eV, as a function of the distance from the surface of a (5,5) nanotube, d, along the x axis. The enhancement is significant out to about 0.8 nm.

$$L(r,\theta,\omega) = \left| \frac{\mathbf{E_0}(r,\theta) + \mathbf{E_{ind}}(r,\theta,\omega)}{\mathbf{E_0}(r,\theta)} \right|. \tag{6}$$

The enhancement at the surfaces of several SWCNTs is plotted in Fig. 5. In this figure, the electric field enhancement is plotted along the axis parallel to the incident electric field on a radial line on the incident side of the CNT. It therefore does not show the θ dependence of the enhancement which has a sinusoidal variation with a maximum at $\theta=0$ and π and a minimum at $\theta=\pi/2$ and $3\pi/2$. The maxima are plotted in Fig. 8. The minima also vary with nanotube radius but never drop below an enhancement of $L=1$. This shows that the Mie resonance in the nanotubes increases the local electric field and hence the local energy density.

It is the field intensity that determines the absorption rate of photons by amorphous carbon, a quantity proportional to E^2, and thus to the enhancement factor squared. This *enhancement intensity factor*, L^2, is plotted as a function of the distance from the nanotube in Fig. 6 for a (3,3) nanotube along the x axis. The dielectric function derived from DFPT was used to generate these data.

The enhancement intensity is the largest ($L^2 \sim 44$) for small tubes and drops rapidly with increasing tube radius. For a given tube, there is a well-defined enhancement peak at the frequency for which the real part of the dielectric function causes the denominator of the potential to go to zero. This is associated with Mie resonances. A second peak becomes dominant, though, for larger nanotubes and is associated with a distinct type of Mie resonance, as discussed below.

Equation (6) indicates that the enhancement intensity exhibits a radial decay proportional to r^{-4}. This is quantified in Fig. 6, where it is clear that a measurable enhancement persists out to ~ 0.8 nm.

D. Resonant frequency

Peaks in the field enhancement are indicative of incident field resonance with a Mie resonance. If the system is assumed to be low loss—i.e., Im(ϵ) is small—the common denominator in Eq. (2) can be set to zero to estimate the conditions for resonance. The result is a relationship between the resonant dielectric function, ϵ_{res}, and the inner and outer radii of the cylinder,

$$\epsilon_{\text{res}} = \frac{a \pm c}{a \mp c}. \tag{7}$$

The resonance associated with a negative sign in the numerator and a positive sign in the denominator will be referred to as *Mie resonance 1* with the other possibility called *Mie resonance 2*. They correspond to constructive and destructive coupling of the electric fields the form the Mie resonance. One solution occurs when the electric fields of these resonance have the same signs (Mie resonance 1) while the other corresponds to the electric fields having opposite signs (Mie resonance 2). This is the cylindrical analog of the Mie resonance associated with the coupled plasmons at the interfaces between thin films.[37] The relevant electric fields for thin films are depicted in Fig. 7. The dielectric constant is negative for both resonant conditions. This is consistent with the requirement that the materials be conducting. Note that the existence of these two localized Mie resonances do not rely on any particular model for the dielectric function.

The Mie resonant frequencies can now be determined. This is accomplished by substituting the relations of Eq. (7) into a frequency-dependent dielectric model. The dielectric response derived by use of DFT was subsequently applied to obtain the resonant frequencies for a range of conducting SWCNTs. However, since the dielectric function is deter-

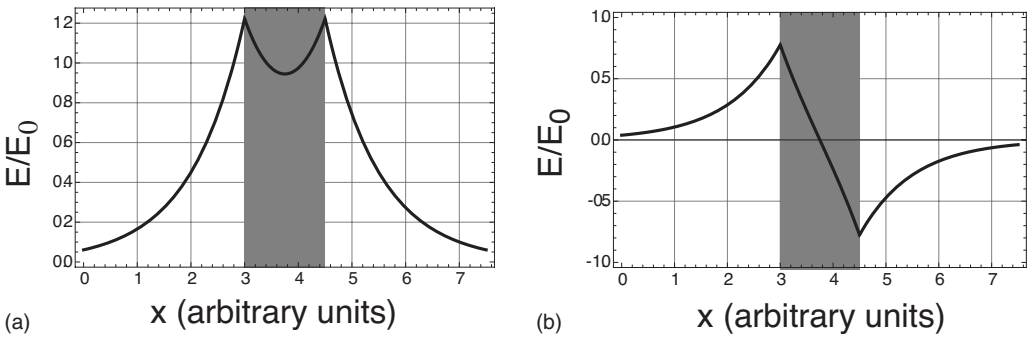

FIG. 7. The two solutions for the electric field in arbitrary units of two Mie resonances in a thin film defined by the gray region. The electric fields have the same sign in (a) and opposite signs in (b).

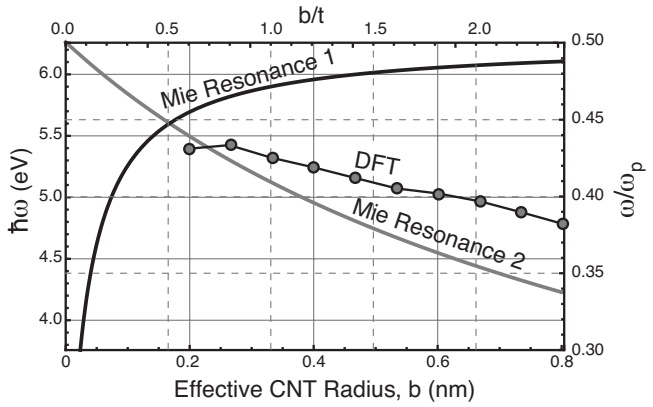

FIG. 8. The resonant frequency obtained from DFT is shown as gray circles with the black curve to guide the eye. The DFT Mie resonance intersects 5 eV for a radius of 0.6 nm. The radius of Carbolex nanotubes is in the range of 0.6–0.7 nm.

mined numerically, the resonant frequency was determined by including the real and imaginary dielectric functions in the square of the electric field enhancement and selecting the frequency associated with the maximum electric field enhancement. The peak that corresponds to Mie resonance 2 is identified in Fig. 5 as the primary resonant peak. The peak corresponding to Mie resonance 1, however, is not seen since ϵ does not cross the corresponding resonant value. The secondary peak seen corresponds to a second Mie resonance 2. This Mie resonance arises because the dielectric function from DFT crosses the resonant frequencies twice. Figure 8 shows a linear correspondence with the radius between the (4,4) nanotube and the (12,12) nanotube for the primary Mie resonance. The nonlinearity associated with the (3,3) nanotube is attributed to the large strain induced by the large curvature.[7]

Mie resonance 1 occurs at more negative values of the dielectric function than is seen in these tubes and therefore does not exist to be able to excite $\pi \rightarrow \pi^*$ transitions in amorphous carbon. The associated electric field is plotted in Fig. 9(a). As shown the electric field of Mie resonance 1 is characterized by destructive interactions between the electric field from the cylinder's surfaces along the direction of incident light (x axis). Mie resonance 2 is shown to occur twice in larger diameter tubes in Fig. 5 due to the dielectric function crossing the resonant value twice. The associated electric field is plotted in Fig. 9(b). Mie resonance 2 exhibits a resonance with the constructive interaction along the x axis.

IV. DISCUSSION

The key step in linking laser cleaning to a-C oxidation lies in understanding the excitation of resonant electrical states in the vicinity of nanotubes. Both polarization and frequency of the incident field must be considered. For instance, radiation polarized along the tube axis will generate collective excitations at all frequencies that are localized near the surface and decay exponentially along radial lines. The quasiparticle appellation for this is a *surface-plasmon polariton* (SPP).[37] If the electric field is polarized perpendicular to the nanotube

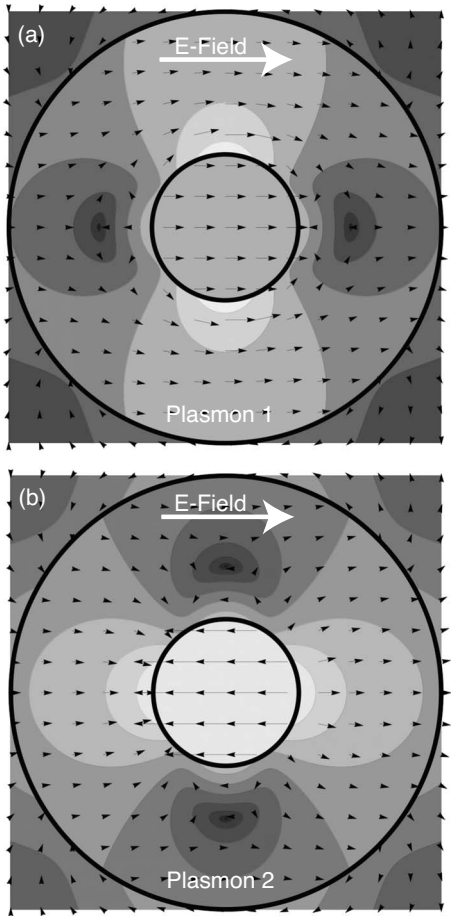

FIG. 9. The electric field in the infinite hollow conducting cylinder with the radius (0.339 nm) of a (5,5) nanotube using the resonant values of ϵ of (a) $\epsilon_{\mathrm{res}}=\frac{a+c}{a-c}=-2.02$ and (b) $\epsilon_{\mathrm{res}}=\frac{a-c}{a+c}=-0.49$. Both resonances have constructive (light) and destructive (dark) interference between the electric fields from the surfaces. The arrows are the electric field direction. Shading represents the magnitude of the electric field with darker representing a stronger field.

axis, though, it is possible to induce collective excitations that are frequency dependent, because they are tied to standing waves formed by conduction electrons wrapping the tube circumference. These excitations, termed *localized* SP (LSP) (Ref. 37) do not decay exponentially with radius but are still localized at the tube surface. The resonance electric field associated with an LSP is a Mie resonance. The result of establishing such a resonant condition is that the local electric field may be significantly amplified over that which is perpendicular to the tube axis. The LSP are a general feature of the closed nature of surfaces and are, for instance, the cornerstone of SERS.[37] A different type of collective excitation has been identified in our current analysis and relies on the coupling of LSPs between inner and outer surfaces of hollow tubules. If the tube shell is sufficiently thin, the inner and outer LSPs will create what we dub a *localized* SPP (LSPP), and this interaction may be either constructive or destructive. Figure 7 shows this constructive and destructive interaction for an LSPP in a thin film but a frequency-dependent LSPP requires a closed boundary in at least one direction.

Figure 9 plots the direction and magnitude of the total electric field (including both applied and induced fields) for a (5,5) tube at the resonant values of the dielectric function. The plots clearly show the electric fields that characterize Mie resonances 1 and 2, which are the electric fields corresponding to the two manifestations of a LSPP. The coupling between the LSP on either surface of the cylindrical shell is evident in the figure. Both of the subfigures in Fig. 9 show regions of constructive and destructive interaction between the electric fields from the plasmons on the two surfaces. Figure 9(a) shows constructive interaction along the direction of the applied field and destructive perpendicular (Mie resonance 1). Figure 9(b) has the opposite orientation (Mie resonance 2). These interactions are due directly to the localized nature of the plasmons which gives rise to the Mie resonance. The direction of the electric field inside the cylindrical shell for both resonances rotates a full 360° in the span of half the cylinder near the inner radius but the initial and final directions for the two resonances are opposite. The rotation of direction for the two resonances dictates where constructive and destructive interactions occur. An azimuthal dependence also exists outside the nanotube but does not significantly effect the enhancement.

Our theoretical results indicate that the SWCNT Mie resonance can result in a locally strong electric field which exposes neighboring a-C to intensities of UV radiation higher than what would be present without the tubes. In order to be useful for cleaning, though, this enhancement has to occur at frequencies to which the a-C is sensitive. Specifically, a-C is known to be photochemically active in the vicinity of 5 eV (Ref. 14) due to the $\pi \rightarrow \pi^*$ transition.[22,23] These bonds are associated with sp^2 bonded carbon atoms and we assume that the a-C to be removed is strongly populated with the requisite structures.[2] Our simple cylindrical model predicts that sufficiently small CNTs will generate an enhanced field in this range, as summarized in Fig. 5. This establishes a link between UV radiation and the activation of sp^2 bonds with a-C.

A relationship between the excitation of sp^2 bonds and a-C removal must still be elucidated. This is the focus of future work on the purification of SWCNTs. However, a brief discussion of the process follows to demonstrate the link between the field enhancement of the nanotubes and the cleaning of a-C. Because our previous experiments show that cleaning relies on oxygen, we conclude that a-C is removed via oxidation. This leaves two possible links between the increased rate of $\pi \rightarrow \pi^*$ transitions and cleaning. Both mechanisms can be most easily considered in terms of the kinetic equation for oxidation of a-C in its excited state,

$$R = [O_2]^n [\text{a-C}^*]^m A e^{-E^*_{\text{act}}/k_b T}. \quad (8)$$

Here R is the rate of cleaning, $[O_2]$ is the concentration of O_2 present, $[\text{a-C}^*]$ is the concentration of the excited π^* state present, n and m are the reaction orders of the reaction, A is the pre-exponential factor, E^*_{act} is the activation energy for the oxidation of a-C in the π^* state, k_b is Boltzmann's constant, and T is the local temperature at which the oxidation occurs. A similar equation exists for oxidation of a-C in its ground state but the activation energy is large enough to make the rate of oxidation negligible.[40] The two possible mechanisms are tied to different components within this equation. A *thermal hypothesis* is that CNTs exposed to pulsed UV light results in rapid and localized temperatures increase [T in Eq. (8)] in the amorphous carbon, which facilitates carbon oxidation. Mie resonance and the associated thermalization may simply heat the surrounding a-C to a point at which the rate of oxidation is enhanced. If this is the case, then the rate of a-C removal should be reproducible by heating pure a-C by other means. An alternative *field enhancement hypothesis* is that the locally enhanced EM field increases the concentration of activated bonds, $[\text{a-C}^*]$. Oxidation would then proceed more rapidly because the rate is proportional to this concentration. Both hypotheses are consistent with our experimental analyses and theoretical modeling. It is likely that both processes occur to some degree and further experimentation is required in order determine their relative importance. In either case, though, the cleaning efficacy is tied to a local field enhancement which results from the excitation of LSPPs. As has been shown, the square of the local field enhancement is nearly 44 times at the nanotube surface and continues to be significant beyond 0.8 nm from the surface.

ACKNOWLEDGMENTS

The authors thank Isaak Mayorgoyz of the University of Maryland EE department for his discussion concerning plasmons. Also, thanks goes to Wu, Wood, Collins, and Furtak of the Colorado School of Mines Physics and Chemical Engineering Departments for their input on plasmons and photochemistry. This research was supported in part by the Golden Energy Computing Organization at the Colorado School of Mines using resources acquired with financial assistance from the National Science Foundation and the National Renewable Energy Laboratory.

[1] Ray H. Baughman, Anvar A. Zakhidov, and Walt A. de Heer, Science **297**, 297 (2002).

[2] *Properties of Amorphous Carbon*, Emis Datareviews Vol. 29, edited by S. R. P. Silva (INSPEC, London, 2003).

[3] R. Saito, G. Dresselhaus, and M. S. Dresselhaus, *Physical Properties of Carbon Nanotubes* (Imperial College Press, Exeter, England, 2003).

[4] Sreejarani K. Pillai, Suprakas Sinha Ray, and Mathew Moodley, J. Nanosci. Nanotechnol. **7**, 3011 (2007).

[5] K. Maehashi, Y. Ohno, K. Inoue, and K. Matsumoto, Appl. Phys. Lett. **85**, 858 (2004).

[6] K. Ramadurai, C. L. Cromer, A. C. Dillon, R. L. Mahajan, and J. H. Lehman, J. Appl. Phys. **105**, 093106 (2009).

[7] Yi-Fan Li, Chia-I. Hung, Ching-Chen Li, Wei Chin, Bee-Yu

Weib, and Wen-Kuang Hsu, J. Mater. Chem. **19**, 6761 (2009).
[8] J. S. Kim, K. S. Ahn, C. O. Kim, and J. P. Hong, Appl. Phys. Lett. **82**, 1607 (2003).
[9] K. E. Hurst, A. C. Dillon, D. A. Keenan, and J. H. Lehman, Chem. Phys. Lett. **433**, 301 (2007).
[10] Katherine E. Hurst, Anne C. Dillon, Shao Yang, and John H. Lehman, J. Phys. Chem. **112**, 16296 (2008).
[11] Brain J. Landi, Herbert J. Ruf, Chris M. Evans, Cory D. Cress, and Ryne P. Raffaelle, J. Phys. Chem. B **109**, 9952 (2005).
[12] J. Yotani, S. Uemura, T. Nagasako, H. Kurachi, H. Yamada, T. Ezaki, T. Maesoba, T. Nakao, M. Ito, T. Ishida, and Y. Saito, Jpn. J. Appl. Phys., Part 2 **43**, L1459 (2004).
[13] G. Singh, P. Rice, K. E. Hurst, J. H. Lehman, and R. L. Mahajan, Appl. Phys. Lett. **91**, 033101 (2007).
[14] Paula E. Colavita, Bin Sun, Kiu-Yuen Tse, and Robert J. Hamers, J. Vac. Sci. Technol. A **26**, 925 (2008).
[15] Yoichi Murakami and Shigeo Maruyama, Phys. Rev. B, **79**, 155445 (2009).
[16] José M. Soler, Emilio Artacho, Julian D. Gale, Alberto García, Javier Junquera, Pablo Ordejón, and Daniel Sánchez-Portal, J. Phys.: Condens. Matter **14**, 2745 (2002).
[17] E. N. Economou, *Green's Functions in Quantum Physics*, Solid-State Science, 3rd ed. (Springer, New York, 2006).
[18] H. Kataura, Y. Kumazawa, Y. Maniwa, I. Umezu, S. Suzuki, Y. Ohtsuka, and Y. Achiba, Synth. Met. **103**, 2555 (1999).
[19] C. Kramberger, R. Hambach, C. Giorgetti, M. H. Rummeli, M. Knupfer, J. Fink, B. Buchner, L. Reining, E. Einarsson, S. Maruyama, F. Sottile, K. Hannewald, V. Olevano, A. G. Marinopoulos, and T. Pichler, Phys. Rev. Lett. **100**, 196803 (2008).
[20] Y. Murakami, E. Einarsson, T. Edamura, and S. Maruyama, Phys. Rev. Lett. **94**, 087402 (2005).
[21] Y. Murakami, E. Einarsson, T. Edamura, and S. Maruyama, Carbon **43**, 2664 (2005).
[22] G. Fanchini and A. Tagliaferro, Diamond Relat. Mater. **10**, 191 (2001).
[23] J. Robertson, Diamond Relat. Mater. **6**, 212 (1997).
[24] U. J. Kim, X. M. Liu, C. A. Furtado, G. Chen, R. Saito, J. Jiang, M. S. Dresselhaus, and P. C. Eklund, Phys. Rev. Lett. **95**, 157402 (2005).
[25] Elisabeth Mansfield, Aparna Kar, and Stephanie Hooker, Anal. Chem. (to be published).
[26] Vasile Mihai Mecea, Anal. Lett. **38**, 753 (2005).
[27] P. Corio, P. S. Santos, M. A. Pimenta, and M. S. Dresselhaus, Chem. Phys. Lett. **360**, 557 (2002).
[28] K. E. Hurst, A. G. Van Der Geest, M. T. Lusk, E. Mansfield, and J. H. Lehman (unpublished).
[29] John H. Lehman, Chaiwat Engtrakul, Thomas Gennett, and Anne C. Dillon, Appl. Opt. **44**, 483 (2005).
[30] T. Dumont, S. Lazare, T. Lippert, and A. Wokaun, Appl. Phys. A: Mater. Sci. Process. **79**, 1271 (2004).
[31] S. Küper, J. Brannon, and K. Brannon, Appl. Phys. A: Mater. Sci. Process. **56**, 43 (1993).
[32] DaJian Wu, XiaDong Xu, and XiaoJun Liu, Solid State Commun. **148**, 163 (2008).
[33] Hendrik J. Monkhorst and James D. Pack, Phys. Rev. B **13**, 5188 (1976).
[34] M. Machon, S. Reich, C. Thomsen, D. Sanchez-Portal, and P. Ordejon, Phys. Rev. B **66**, 155410 (2002).
[35] A. G. Marinopoulos, L. Reining, A. Rubio, and N. Vast, Phys. Rev. Lett. **91**, 046402 (2003).
[36] H. Xu, E. J. Bjerneld, M. Käll, and L. Börjesson, Phys. Rev. Lett. **83**, 4357 (1999).
[37] Stefen Alexander Maier, *Plasmonics: Fundamentals and Applications* (Springer, New York, 2007).
[38] Robert G. Parr and Weitao Yang, *Density-Functional Theory of Atoms and Molecules*, International Series of Monographs on Chemistry Vol. 16 (Oxford Science, New York, 1989).
[39] Richard M. Martin, *Electronic Structure: Basic Theory and Practical Methods* (Cambridge University Press, Cambridge, England, 2004).
[40] Roman Brukh and Somenath Mitra, J. Mater. Chem. **17**, 619 (2007).